Journal of Physics and Chemistry of Solids 133 (2019) 187–196

Contents lists available at ScienceDirect

Journal of Physics and Chemistry of Solids

journal homepage: www.elsevier.com/locate/jpcs

Extension schemes of the dielectric function, and their implications for ion stopping calculations

M. Vos[a,*], P.L. Grande[b]

[a] Department of Electronic Materials Engineering, Research School of Physics and Engineering, The Australian National University, Canberra, Australia
[b] Instituto de Fsica, Universidade Federal do Rio Grande do Sul, Porto Alegre, RS, Brazil

ARTICLE INFO

Keywords:
Ion stopping
Dielectric function
Lithium

ABSTRACT

The dielectric function is often known in the optical limit (zero momentum) but knowledge away from zero momentum is required for the calculation of many physical properties, such as ion stopping and inelastic mean free path. We review the several extension schemes and compare the results with the available literature and investigate in particular the effect of the extension scheme on the calculated proton stopping for the case of Li.

1. Introduction

The interaction of fast, charged particles with matter has been a central topic of research for a long time. Bohr used it to test his emerging understanding of the quantum nature of matter [1], Bethe derived a first description, fully consistent with modern quantum physics [2], and further refinements were due to Lindhard [3], to name only the major players. Besides its fundamental interest the topic is studied for its importance in technological fields like ion beam analysis and ion beam modification of materials. More recently, it has attracted attention within the context of ion-beam based cancer therapy. The field has been thoroughly reviewed by Sigmund [4] and is described in the context of materials science by Nastasi et al. [5], and in the context of medical physics by Nikjoo et al. [6].

In the first Born approximation (FBA) the interaction between projectile and target is considered weak. This is the case when the charge of the projectile is small and its velocity is large. Then one is in the linear regime and first order perturbation theory should suffice. The projectile can then be described as a plane wave and cross sections are proportional to the square of its charge. Under these conditions ion stopping can then be described in terms of the momentum (q) and energy (ω)-dependent dielectric function $\varepsilon(q, \omega)$ [4,7]. The passing of the ion causes an electric field in the target that changes rapidly with position and time. This changing field can be decomposed into Fourier components, with a time and space dependence depending on ω and q. From $\varepsilon(q, \omega)$ the polarization of the target, as a response to this electric field, is calculated and the induced field at the position of the projectile leads to a slowing down of the projectile. Within this framework obtaining the right stopping values requires knowledge of $\varepsilon(q, \omega)$ (or equivalently knowledge of Im $[-1/\varepsilon(q, \omega)]$), but generally, there are no experimental data or ab-initio calculations of this quantity, especially away from $q = 0$. Therefore, model dielectric functions are often employed.

An overview of a variety of model dielectric functions used in the literature was given by Nikjoo et al. [7] and within the contest of proton stopping in water by Emfietzoglou et al. [8]. The effect of calculating the dielectric function beyond the random phase approximation is discussed in Ref. [9]. Novel approaches of including the q-dependence to the dielectric function were discussed by Chantler and Bourke [10,11] will not be considered here. The dielectric function is used in track simulation of protons and electrons for charged particle dosimetry e.g. Refs. [12,13].

We want to study how ion stopping depends on the extension scheme used for the dielectric function away from q = 0 and address several important questions:

- What are the consequences of adopting various models for the extension of $\varepsilon(q, \omega)$ for $q \neq 0$, for the calculation of ion stopping?
  -Can we explore spectroscopic techniques to test the validity of various extension schemes?
  -Can we estimate how the stopping changes if we use calculations that go beyond the linear regime ? These corrections should become important at lower projectile velocities v where the projectile presents a large perturbation of the target system.

We aim to keep the discussion as simple as possible and will only consider proton stopping, to avoid largely the problems due to different charge states, and assume that the projectile velocity is low enough for

* Corresponding author.
E-mail address: maarten.vos@anu.edu.au (M. Vos).

https://doi.org/10.1016/j.jpcs.2019.03.010
Received 7 December 2018; Received in revised form 8 March 2019; Accepted 10 March 2019
Available online 14 March 2019

relativistic effects to be neglected. Unless otherwise stated we use atomic units.

2. Dielectric formalism

The dielectric theory is a well-established way of describing the interaction of charged particles with matter [3,14]. It is a first Born theory i.e. it assumes weak interaction of the projectile with the target. Central to describing the interaction of the projectile with the target is the imaginary part of the inverse dielectric function. The probability that the projectile creates an excitation with momentum q and energy ω per unit path length travelled is proportional to the energy loss function (ELF): Im $[-1/\varepsilon(q, \omega)]$ The kinetic energy and momentum of the projectile will change accordingly. The stopping force on a proton with energy E_0 and mass M can be expressed in terms of the ELF:

$$-\frac{dE}{dx} = \frac{2Z^2}{\pi v^2}\int_0^\infty \frac{dq}{q}\int_0^{qv} \omega\, d\omega\, \mathrm{Im}\left[\frac{-1}{\varepsilon(q,\omega)}\right], \tag{1}$$

with $v = \sqrt{2E_0/M}$ the ion speed and Z the charge of the projectile. We usually consider $Z = 1$ (ionized protons).

Im $[-1/\varepsilon(q, \omega)]$ is a property of the target and has often been determined experimentally in the optical limit ($q = 0$). Calculation of ion stopping requires integration over a large part of (q, ω) space and does thus depend on the assumptions on how the dielectric function can be extended for $q \neq 0$.

A very simple description of a solid (Drude model) considers electrons as classical particles and assumes the nuclei can be described by a uniform positively charged background. In such a target the electrons (with density n) would have collective excitation modes ('plasmons') and the dielectric function (at $q = 0$) can be described as [15]:

$$\varepsilon(\omega) = \varepsilon_1 + i\varepsilon_2 = 1 - \frac{\omega_p^2}{\omega^2 + \Gamma^2} + \frac{i\Gamma\omega_p^2}{\omega(\omega^2 + \Gamma^2)} \tag{2}$$

and the corresponding ELF:

$$\mathrm{Im}\left[\frac{-1}{\varepsilon(\omega)}\right] = \frac{\omega\Gamma\omega_p^2}{(\omega^2 - \omega_p^2)^2 + (\omega\Gamma)^2} \tag{3}$$

with $\omega_p = \sqrt{4\pi n}$ the plasmon frequency and Γ the damping constant. Experimentally it is known that the plasmon energy depends on q, e.g. from electron energy loss measurements [15]. Hence we have to add a q dependence. The argument usually made is that at large q the projectile interacts with a single electron at a time and the energy of the final state (and thus the energy loss) should approach the free particle value: $q^2/2$. Thus often the 'simple quadratic dispersion' is introduced: $\omega_p(q) = \omega_p(0) + q^2/2$. Then the stopping values for protons can be calculated be integrating eq. (1). For an oscillator with $\omega_p(0) = 15$ eV a maximum in the stopping power is found near $E_0 = 20$ keV as shown in Fig. 1. Note also that the stopping is very small if the dispersion curve is, for all q values, at energies larger than qv as the integration over energy in eq. (1) is only up to qv. Indeed under these conditions the stopping vanishes completely if Γ is taken to be zero.

Changing the dispersion will thus change the calculated stopping value. Another frequently used choice is 'full dispersion': $\omega_p(q)^2 = \omega_p(0)^2 + \frac{2}{3}q^2E_F + q^4/4$ with E_F the Fermi energy. In that case the dielectric function is the plasmon-pole approximation [16] to the Lindhard dielectric function [3]. As can be seen in Fig. 1 such dispersion relation means the plasmon energy changes slightly slower with q and, as a consequence, the onset of the stopping starts at smaller E_0 values and the stopping near the maximum is slightly larger.

One of the earliest estimates of the ion stopping was by Bethe [2]. He obtained the stopping by considering soft (small q) and hard (large q) collisions. For an electron gas system Lindhard [3] obtained the Bethe-like stopping formula for protons:

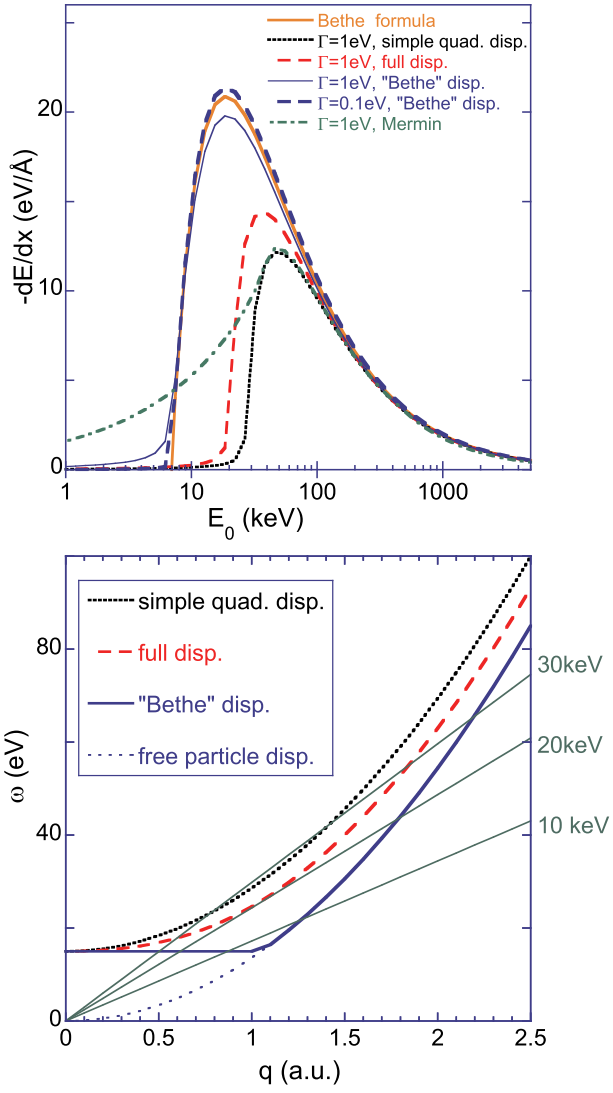

Fig. 1. The stopping curve for a solid with a plasmon at 15 eV for the models as indicated (top), as well as the dispersion used in these models (bottom). There is only contribution to the stopping when the qv line (shown for E_0 = 10, 20 and 30 keV) is above the dispersion curve for some q.

$$-\frac{dE}{dx} = \frac{4\pi n Z^2}{v^2}\ln\left(\frac{2v^2}{\omega_p}\right). \tag{4}$$

This is plotted in Fig. 1 as well. Clearly the onset in Bethe's formula is at even lower energies than obtained for simple quadratic and full dispersion, and the maximum stopping value is larger. As shown in the appendix, if we change the dispersion used in the simple Drude model, described above to:

$$\omega_p(q) = \max\left(\omega_p, \frac{q^2}{2}\right), \tag{5}$$

then, in the limit of small damping ($\Gamma \to 0$) one recovers stopping values of eq. (4).

Lindhard derived $\varepsilon_L(q, \omega, \omega_p)$, a dielectric function for free-electron gas, based on quantum physics by considering all possible excitations from electrons within the Fermi sphere. He found contributions to the ELF due to plasmon excitations, concentrated along a line in (q, ω) space, and due to electron-hole pair excitations covering an area of (q, ω) space that can be derived from simple energy and momentum conservation arguments. Mermin added a relaxation time to the excitations giving a finite width to the plasmon branch [17]. Such a

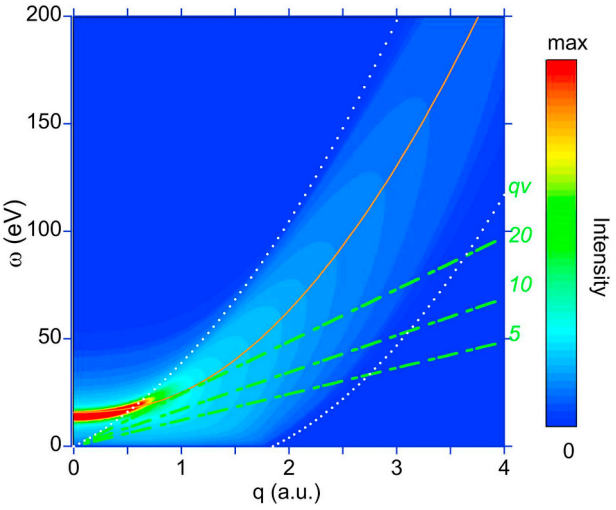

Fig. 2. Im $[-1/\varepsilon(q, \omega)]$ of the Mermin dielectric function (Lindhard dielectric function + relaxation time) plotted for an electron gas with the same density as Al (ω_p = 15 eV). Besides the plasmon branch, similar to what is seen in the Drude dielectric function, there is also intensity due to electron-hole excitation (in between the white dash-dotted lines). The qv lines are shown for E_0 = 5,10 and 20 keV.

Mermin loss function is shown in Fig. 2 for the electron density of Li metal. For small q values the dielectric function is very similar to the Drude dielectric function, but at larger q values the contribution of electron-hole pairs can be seen clearly. A significant consequence of this is that for any projectile velocity v there is always some intensity of the ELF below the qv line and the stopping is thus never zero. Note that in the Mermin model the dispersion is built-in and at any q the ω value with maximum intensity follows the 'full dispersion' closely. The Drude dielectric function predicts a threshold projectile energy, below which there is virtually no stopping. This is not observed experimentally. Within the Mermin approach there is no such threshold. Therefore, we will mainly consider the Mermin dielectric function in the following.

There are sum rules that should apply to any dielectric function. For example, there is the f-sum rule:

$$\frac{1}{2\pi^2}\int_0^\infty \omega' \mathrm{Im}[\varepsilon(q, \omega')]d\omega' = n, \tag{6}$$

which should be fulfilled at any q. Similarly the Bethe sum rule:

$$\frac{1}{2\pi^2}\int_0^\infty \omega' \mathrm{Im}\left[\frac{-1}{\varepsilon(q, \omega')}\right]d\omega' = n, \tag{7}$$

Causality implies that the real and imaginary part of $\varepsilon(k, \omega)$ are linked via Kramers-Kronig relations:

$$\varepsilon_1(q, \omega) - 1 = \frac{2}{\pi}\mathscr{P}\int_0^\infty \frac{\omega'\varepsilon_2(q, \omega')}{(\omega')^2 - \omega^2}d\omega' \tag{8}$$

with $\mathscr{P}$ the Cauchy principal value. Re $[1/\varepsilon(q, \omega)]$ and Im $[1/\varepsilon(q, \omega)]$ are Kramers-Kronig pairs as well. The Mermin dielectric function fulfills all these sum rules. Some different approaches to the calculation of the stopping from the dielectric function were discussed by Pathak and Yussouff [18] and Kaneko [19].

3. Real solids

3.1. Describing long tails

For real solids the ELF in the optical limit has more structure than just a single plasmon peak. Even for free electron metals there are core-level related features in the ELF at ω values close to their binding energies. In many cases these core electrons contribute significantly to ion stopping. Therefore Abril et al. [20] suggested to describe the ELF in the optical limit as a sum of Mermin dielectric functions each with weight A_i, energy ω_i and width Γ_i. By choosing the energy width and weight of each component appropriately one can approach the measured ELF at $q = 0$ and check, using the Bethe sum rule that the total electron density is correct. The use of Mermin function implies that, if the sum rule is fulfilled at $q = 0$, it is adhered to at all q values. Moreover, as long as $\sum_i A_i = 1$ the real and imaginary part of the sum of Mermin functions are indeed Kramers-Kronig pairs.

The question now arises if this decomposition is unique, at least in the sense that for two good-quality fits of the ELF at $q = 0$ the extracted observables (e.g. ion stopping) are very similar. Let us consider the case of Cu. Here Abril et al. [20] obtained a good fit of the ELF at $q = 0$ using 5 components. One of the components with ω_i = 79 eV, describes the strong tail of the Cu ELF at high ω values and is very wide (Γ_i = 152 eV). This component is quite strong, it contributes to the Bethe sum more than half of the total. It is, of course, possible to obtain a good fit using more components, each with a smaller width but with a range of ω_i values. Would such a fit lead to the same proton stopping?

To investigate this, we took *only* this Mermin component and fitted it with a number of Mermin functions, for $q = 0$ each with different ω_i and Γ_i value. As can be seen in Fig. 3 a very similar shape is obtained with a larger number of components. Interestingly, the calculated stopping values differ significantly for smaller proton energies. It

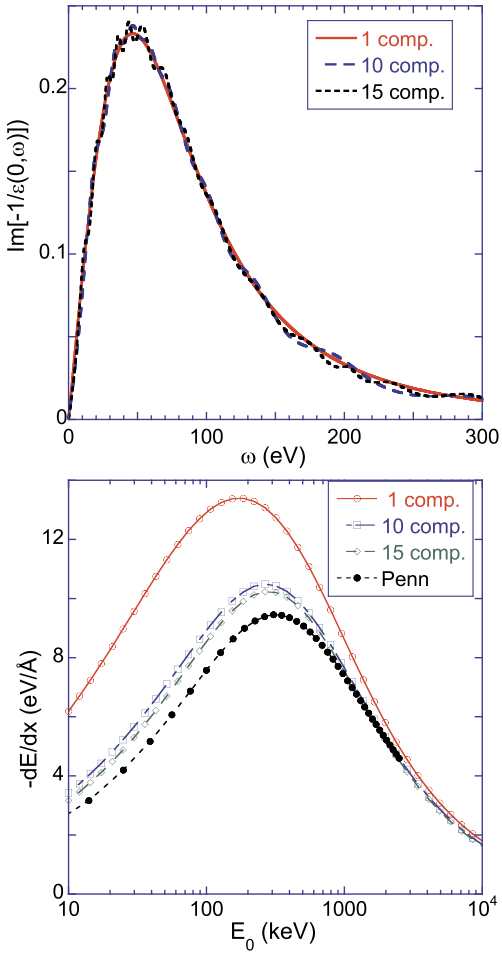

Fig. 3. A single Mermin (ω_1 = 79 eV) with a very large width (Γ_1 = 152 eV) at q = 0 fitted as the sum of 10 and 15 more narrow Mermin loss functions (top) and the derived stopping values for protons (bottom). Although the description in the optical limit is very similar, the calculated stopping differs significantly for smaller projectile energies.(The exact parameters used in the calculation are given in the supplementary materials.)

decreases by more than a factor of 1.5 if 15 components are used compared to a single one.

One could fit the loss function with even more components, with even smaller width. In the limit that $\Gamma \rightarrow 0$ the procedure approaches the one used by Tung et al. [21] and Penn [22] based on the Lindhard dielectric function:

$$\mathrm{Im}\left[\frac{-1}{\varepsilon(q,\omega)}\right] = \int_0^\infty d\omega_p g(\omega_p)\mathrm{Im}\left[\frac{-1}{\varepsilon_L(q,\omega,\omega_p)}\right] \quad (9)$$

with

$$g(\omega) = \frac{2}{\pi\omega}\mathrm{Im}\left[\frac{-1}{\varepsilon(0,\omega)}\right]. \quad (10)$$

The factor $2/(\pi\omega)$ reflects the fact that the ELF from the Lindhard dielectric function (see eq. (9)) has, at $q = 0$, the shape of a delta function but with area $\pi\omega/2$. The obtained stopping values of this 'Penn' procedure are shown in Fig. 3 as well. The obtained Penn stopping values are even slightly less than the fit with 15 Mermin components.

The main differences in the stopping caused by the tail component is for $E_0 < 1$ MeV. For the case of copper the main contribution to the stopping below $E_0 = 1$ MeV is from the outer valence electrons modelled by Abril et al. [20] with oscillators with $\omega_i < 50$ eV. A fit of the tail of the Cu ELF with narrower components would reduce the overall stopping of protons in Cu below 0.3 MeV by 10–15%.

The reason that the stopping values are different becomes obvious when one plots the ELF's at different $q-$values. This is done in Fig. 4 where we compare the single-component ELF to the Penn ELF. At $q = 0$ both are the same (by construction) but at larger q values the single broad Mermin is larger at smaller ω-values than the corresponding Penn ELF (or the ELF from the 10 of 15 component fit). Hence there is more intensity below the $q\nu$-line at smaller E_0 values, leading to a larger stopping. As both approaches have the same Bethe sum (eq. (7)) for all q, both curves necessarily cross and the Penn approach has a tail with larger intensity. This ensures that, in the high E_0 limit both approaches give the same stopping. Similar observations can be found in the recent paper by Da et al. studying the dielectric function in the context of the inelastic mean free path [23].

Which stopping result is the correct one? The relaxation time in the Mermin model is related to the rate at which the excited state decays. Assume, for simplicity, that the final state can be described as a nearly free electron with an energy near 100 eV. For a 100 eV electron (velocity 2.7 a.u.) the inelastic mean-free-path is of the order of 10 a.u.,

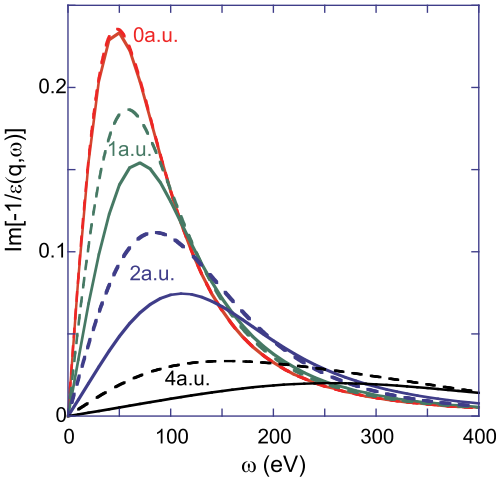

Fig. 4. A comparison of $\mathrm{Im}\,[-1/\varepsilon(q,\omega)]$ at the q values as indicated for a single broad Mermin oscillator ($\omega_1 = 79$ eV, $\Gamma_1 = 152$ eV) (dashed line) and its description using the Penn approach (solid line). At $q = 0$ both approaches coincide.

corresponding to a lifetime of 10/2.7 = 3.7 a.u. And hence a width () of 1/3 a.u., corresponding to 7eV. Clearly a Γ value of 152 eV is too large. The large tail is better interpreted as a consequence of the presence of a range of electron densities in Cu (and hence a range of plasmon energies resulting together in a long tail) and hence the fit with narrower components (or the Penn approach) seems more reasonable. We conclude that the use of very broad Mermin functions in the description of the ELF will result in too large stopping values at low E_0.

3.2. Describing edges

Another difficulty one encounters when one wants to describe the optical ELF by a sum of Mermin ELFs is the presence of sharp edges at energies where excitation of core levels becomes possible. Obtaining a good fit of the sharp edge requires a very large number of Mermin functions (making the method more computational expensive). Therefore other solutions have been suggested in the literature.

Abril et al. fitted the ELF with Mermins, some of them were truncated at the edge energy ω_{edge}, obtaining the sharp edge in this way. Good fits of the optical ELF are easily obtained in this way [20]. Simple truncating the Mermin dielectric function at the same energy for all q-values would result in a Bethe sum with n values that depends on q. To retrieve the right n value for all q Abril et al. made the truncation energy $q-$ dependent: $\omega_{edge}(q)$ and adjusted the edge energy so the Bethe sum gives the same result at all q [20]. In practice this results in the truncation energy increasing with q. For deeper edges, where solid-state effects are small, Heredia-Avalos et al. suggested the use of generalised optical oscillators (GOS) as can be calculated for isolated atoms, e. g based on hydrogenic wave functions [24]. The GOS approach ensures satisfying the Bethe sum at all q.

In a previous work we suggested as an alternative to keep the truncation energy constant but vary the amplitude A with which the oscillator contributes to the dielectric function with q in a way that the Bethe sum is fulfilled at all q. We compared the $\omega_{edge}(q)$ and this $A(q)$ method extensively before [25]. Here we restrict ourselves to the $A(q)$ method.

Da et al. used a third approach. They fitted the dielectric function with Mermin functions only, but allowed for oscillators with both positive *and* negative intensity [26,27]. This makes it possible to create sharp edges with a manageable number of Mermin functions. Using this method the Bethe sum is fulfilled automatically at all q. We will refer to this approach as the 'negative A' method.

Finally one can use the Penn method to obtain the dielectric function for all (q,ω) values from the ELF. This is computationally expensive but avoids any curve fitting and its ambiguities.

To highlight the differences between all approaches we calculated the GOS at $q = 0$ for a Li 1s level with an onset near 55 eV and analysed this with the various approaches (see Fig. 5). The GOS was calculated following the procedure described in Ref. [24] and had a sharp onset near 55eV. We fitted GOS at $q = 0$ with the $A(q)$ method and the negative A method and obtained a reasonable fit. The Penn method gives a perfect description at $q = 0$ by construction. Then we calculated the contribution to the energy loss function at several other q values. The results vary greatly. Both the Penn method and the negative A method have the edge dispersing to larger ω values for small q and the edge disappears at larger q, being replaced by a gradual increasing intensity, starting from $\omega = 0$. This is not physical as the energy loss should be at least the core level binding energy. The GOS and $A(q)$ method maintain an edge at the same position as at $q = 0$ but the intensity of the GOS method near the edge is, away from $q = 0$ larger than the $A(q)$ method. Again all ELF curves have the same Bethe sum, so they necessarily cross. The derived stopping curves are shown in Fig. 6, the absolute values are of course determined by the density of atoms assumed in the model system. The negative A and Penn method do not have a threshold value above which the stopping becomes appreciable, as their ELF have for large q (unrealistic) intensity for small ω values. The GOS has the

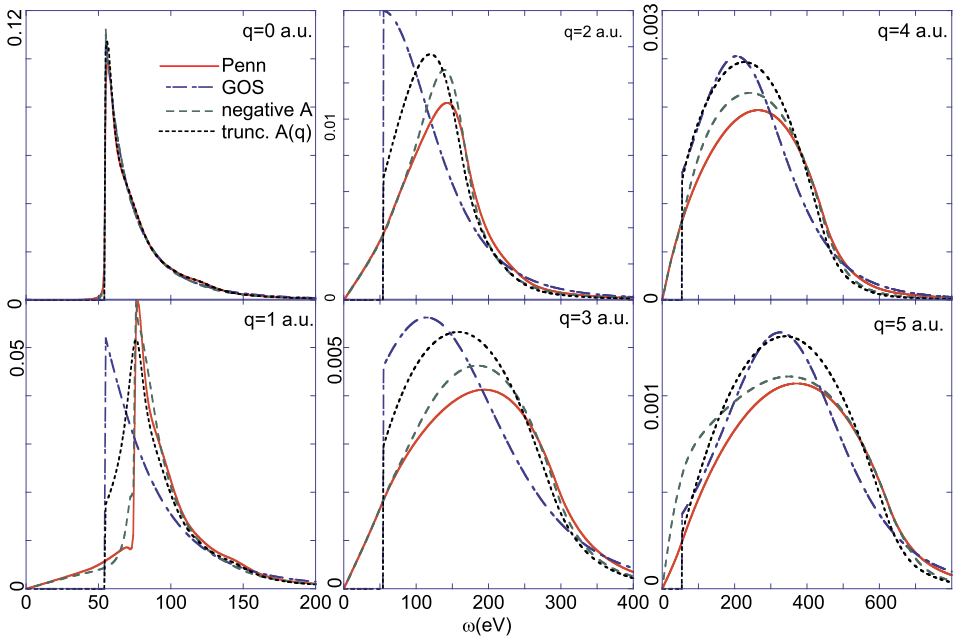

Fig. 5. Model calculations for the development of the ELF of the Li 1s level as a function of q for the models as indicated.(The exact parameters used in the calculation are given in the supplementary materials.)

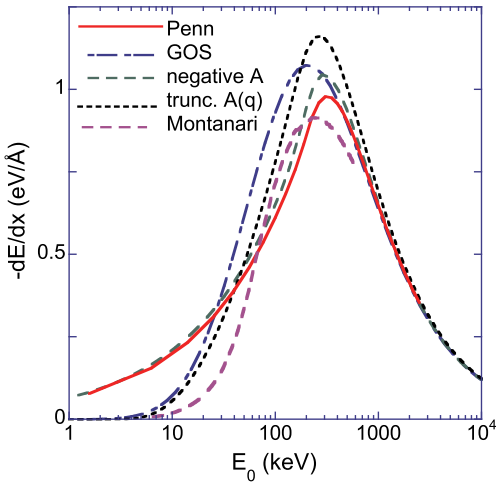

Fig. 6. The derived stopping curves for the model core level for the various extension methods as indicated as well as the Li 1s stopping power as calculated by Montanari and Miraglia [28].

largest value of the ELF just above 55 eV and hence it has the largest stopping value for $E_0 \approx 100 - 200$ keV. For large E_0 values all stopping values converge to the Bethe formula result.

Montanari and Miraglia [28] calculated the 1s stopping using the shellwise local plasma approximation based on the Levine-Louie (LL) dielectric function [29]. It is shown in Fig. 6 as well and has an onset of the stopping at larger projectile energies than the other models. In that case the contribution of a core electron level to the ELF is taken as a delta function (with the appropriate area) at the core hole binding energy (which is taken to be the band gap of the LL dielectric function), and no attempt is made to fit the optical ELF. Vos and Grande discussed the use of the Levine-Louie dielectric function plus relaxation time (Mermin-Levine-Louie or MLL) [30] but found that fitting of an ELF with inner shell edges with the MLL has similar complications as the fitting with a Mermin dielectric function. At larger q values the MLL dielectric function (Fig. 3 of ref. [30]) remains very small at ω values below the core level energy (in contrast to negative A and Penn approach) and no sharp increase at the edge position is observed (in contrast to the GOS and A(q) method. The intensity in the shellwise local plasma approximation is thus concentrated at larger ω values explaining its slower onset with increasing projectile energy.

4. Lithium

4.1. Stopping in the linear regime

Now we want to illustrate the various effects discussed for one of most simple cases: lithium metal. It should be reasonably close to a free-electron metal and has only a single core level. Experimental proton stopping data exist [31,32] and this case has been studied theoretically by Mathar et al. [33] and Montanari et al. [28]. We will first neglect charge exchange effects which become important at lower energies and were extensively discussed by Cabrera-Trujillo et al. [34] for *atomic* Li. We will compare the ELF at specific q values with the inelastic X-ray data as measured by Nagasawa et al. [35,36] and high-resolution Compton measurements by Chen et al. [37].

First we need to establish a reasonable estimate for the ELF in the optical limit. For the valence band we can use the optical result of Rasigni et al. [38], which gives for the plasmon energy 7.0 eV (maximum intensity of the optical ELF) in good agreement with (transmission) electron energy loss measurements of ref. [39] (7.08 eV). This is less than the calculated plasmon energy, assuming 1 free electrons per Li atom (8.0 eV) indicating that a plasmon at 7 eV does not account for all Li valence electrons and that band structure effects are significant. Unfortunately there appears to be no optical data for Li beyond 10 eV. To account for all Li valence electrons we take for the plasmon at 7 eV $A_i = 0.8$ and added another broader (4 eV wide) oscillator at 11 eV with intensity $A_i = 0.183$. (Note that the sum of these two amplitude is slightly less than 1 to allow for the contribution of the core level to the Kramers Kronig transform).

At larger energy losses ($\omega > 30$ eV) we use the data of Henke [40] to help us establish the ELF. We obtain a reasonable fit of the 1s ELF structure from Henke (edge at 55 eV) using either 4 truncated Mermin loss functions or a combination of oscillators with positive A_i values and another 4 with negative A_i values.

There are some complications using the GOS approach for shallow

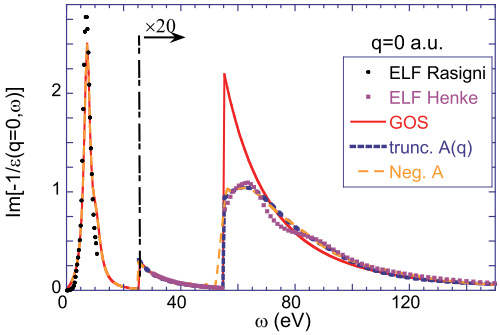

Fig. 7. The ELF at q = 0 from the data from Rasigni and Rasigni [38] and Henke et al. [40] and their description using 3 different model ELF's. For the Penn calculations we assumed it to be identical with the $A(q)$ method at $q = 0$. (The exact parameters used in the calculation are given in the supplementary materials.)

core levels. The predicted edge position, based on Slater effective charges [41] can be different from the actual observed one, and the model does not describe excitations to bound states. To describe the ELF we calculate the GOS starting not from the theoretical edge position but from the actually observed edge position. This affects the area of the GOS, and we apply a $q-$ dependent scaling factor so the right number of electrons (2 electrons per atom for Li 1s) is derived from the Bethe sum rule. The results of the fit for the ELF are shown in Fig. 7.

We also used the Penn approach to calculate the dielectric function at various q values and the stopping. Here we took the ELF at $q = 0$ of the truncated $A(q)$ method as the ELF that defined the Penn dielectric function at all q via eq. (9).

For Li there exist inelastic X-ray scattering (IXS) results by Nagasawa et al. [35,36] that can be compared to the calculated ELF at specific q values. IXS measures the dynamical structure factor $S(q, \omega)$ that is related to the loss function by:

$$S(q, \omega) = \frac{q^2}{4\pi^2 n}\mathrm{Im}\left[\frac{-1}{\varepsilon(q, \omega)}\right]. \tag{11}$$

We compare in Fig. 8 our energy loss functions at $q = 0.59$ a.u. with IXS results from Ref. [35], and our energy loss function at 3.1 a.u. and 4.1 a.u. with those published in Ref. [36].

Many of the trends shown in these experimental spectra are reproduced by the calculations but there are also distinct differences. For the GOS, truncated $A(q)$ and negative A model the valence band loss feature is described identically as the same valence band oscillators are used. The Penn dispersion is somewhat larger (in agreement with our findings in section 3.1. The experimental dispersion at $q = 0.59$ a.u. (about 2 eV) is significantly smaller than the dispersion predicted using the Mermin dielectric function (3.5 eV). As we saw in Fig. 1 this means that the actual stopping for low projectile energies should be larger than calculated from these dielectric functions. For the K edge region at $q = 0.59$ a.u. It is obvious that experimentally the position of the K edge does not depend on q whereas the position within the Penn and Negative A model does increase with q.

For the larger momentum transfers studied ($q = 3.1$ and 4.1 a.u.) the behaviour of the valence electrons approaches the Compton limit, i.e. their contribution is centered at $q^2/2$ (130 eV for q = 3.1 a.u., 230 eV for q = 4.1 a. u.) and the width increases linearly with q. The 1s contribution becomes very broad and extends from the edge over several hundred eV. Experimentally the K edge remains distinct and at the same energy. In the calculations there is substantial difference how their intensity is distributed over ω in the various models. The edge disappears at large q values for the negative A model and the Penn approach and the ELF extends then all the way to $\omega = 0$. The edge of the truncated $A(q)$ model stays, by definition at the same ω value. The original model by Abril et al. [20] that makes the truncation energy a

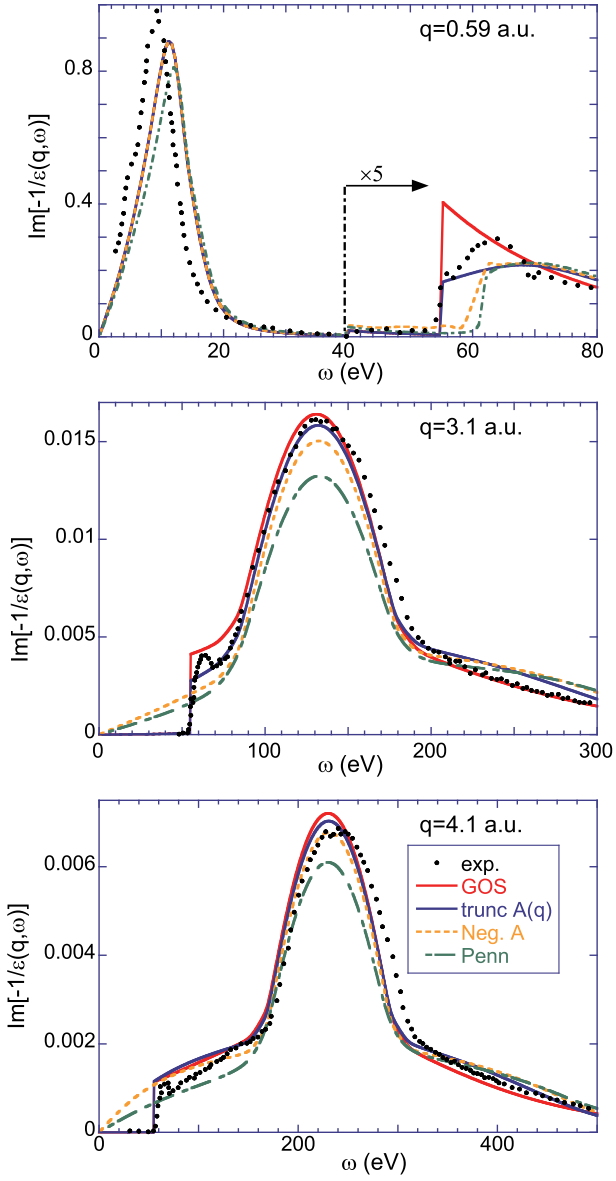

Fig. 8. A comparison with the calculated energy loss function at q values as indicated compared to the inelastic x-ray scattering results. For the Li 1s level four different ways were used to describe its contribution to the ELF (GOS formula, fitting with truncated Mermin, and fitting with both positive and negative Mermin contributions as well as the Penn approach). Note that the Mermin approach gives a dispersion of the plasmon feature at 0.59 a.u. That differs from the experiment. Also the position of the edge remains clear at larger q in the experiment, but the edge disappears in the negative A and Penn approach.

function of q would see the edge shift significantly to larger ω values.

At even larger q values the 1s electrons can also be treated in the Compton limit. In Fig. 9 we show a Compton profile, as measured by Chen et al. [37] and compare it with the dielectric function as calculated for $q = 10$ a.u. At these high momentum transfers it is a reasonable approximation to assume one interacts with only one electron and its final state can be considered a free electron. Then the energy loss (shown on the top) axis and the momentum of the electron *before* the collision (lower axis) $\boldsymbol{p}$ are related as [42]:

$$\omega = \frac{q^2}{2} + \boldsymbol{q}\cdot\boldsymbol{p}, \tag{12}$$

i.e. the energy loss is that of scattering from a free electron *plus* a Doppler broadening term due to the movement of that electron.

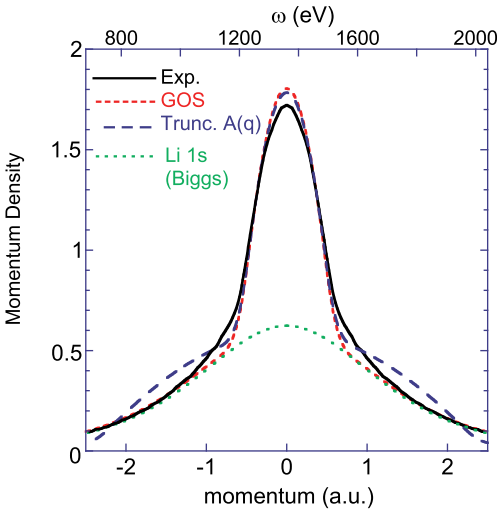

Fig. 9. A comparison with the dielectric function in the high $-q$ limit with the Compton profile as measured by Chen et al. [37]. The calculations were convoluted with the experimental resolution or the Compton measurement (0.16 a.u. FWHM). The 1s contribution, as obtained from a Hartree-Fock calculation by Biggs et al. [43] for atomic Li is shown as well. The energy loss and target electron momentum are related by eq. (12) and here we assumed that q = 10 a.u.

The Compton profile consists of a contribution of the (almost free electron-like) 2s electrons and the atomic 1s electrons. The Compton profile of a free-electron gas resembles an inverted parabola and extends up to k_F the Fermi wave vector (0.325 a.u. For Li), whereas the Compton profile of the 1s electron is broader and does not have a sharp cut-off. For comparison we show the calculated 1s Compton profile from Biggs et al. [43] as well. Note that the GOS approach describes the 1s contribution much better, then the truncated $A(q)$ method or any of the other approaches based on the Mermin loss function (not shown). The 2s contribution is narrower in the calculations as the theory neglects broadening due to the influence of the lattice [33] and electron correlation effects beyond the RPA [44].

4.2. Stopping beyond the linear regime

Non-perturbative treatments of the stopping power are possible by considering the problem from the reference frame where the projectile is at rest. In this frame the projectile interacts with (relatively fast) electrons with a velocity distribution centered around $-v$. The interaction of fast electrons with an atom can be solved exactly assuming a central potential for the ion-electron interaction through the partial wave analysis approach. Once this interaction is calculated, the stopping of the ion in the laboratory frame can be obtained. The standard approach to do that relies on the transport cross section (TCS) which only converges very slowly to the Bethe stopping value at large energies [45]. A property of perturbative (linear) stopping power calculations is that the stopping is proportional to Z^2. In non-perturbative calculations contributions proportional to Z^3, Z^4 etc. Appear. We refer to the terms proportional to Z^3 as the Barkas contribution [46]. Recently, a new non-perturbative formula was derived by Grande [47] that calculates the stopping $((dE/dx)_{IDA})$ using the induced (charge) density (induced density approximation or IDA) for an electron gas and this solution converges to the Bethe limit for large projectile energies much faster.

Incorporating these effects for non-free electron materials one decomposes the target as the sum of electron gases with different densities as described for the Penn method, using eq. (9):

$$\frac{dE}{dx}(v) = \int_0^\infty d\omega_p \, g(\omega_p) \left(\frac{dE}{dx}\right)_{IDA} (v, \omega_p), \tag{13}$$

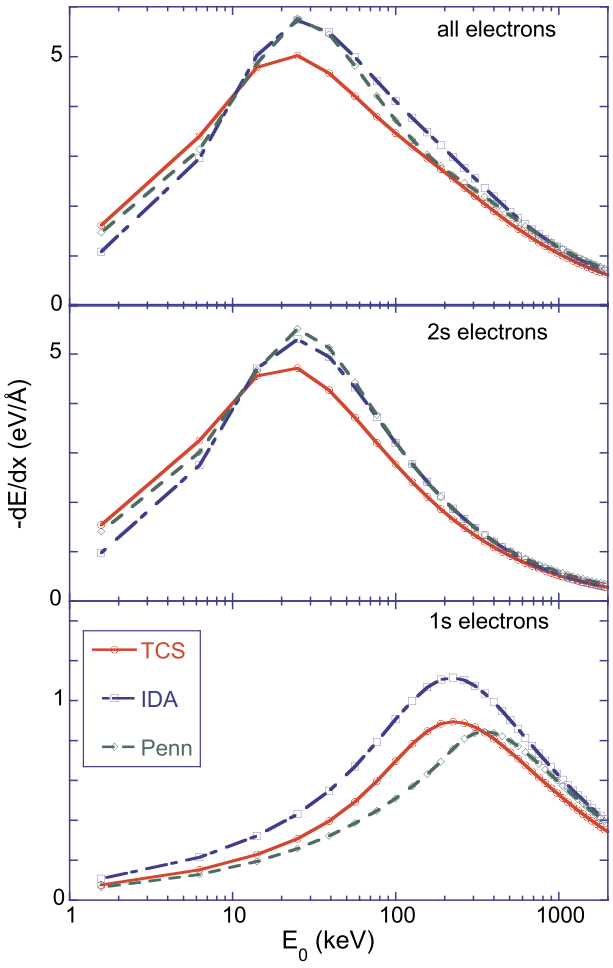

Fig. 10. The total (upper panel) and the contribution to the stopping power of the 2s (central panel) and 1s (lower panel) electrons of Li using the Penn approach ('Penn') and based on the same decomposition into contributions of electron gas of different densities, but now using two non-pertubative approaches to the calculation of the stopping of these electron gases.

where the function $g(\omega)$ defined in Eq. (10) is from the Penn model. The stopping in the IDA (or TCS) approximation of an actual material, is then considered to be the weighted sum of the IDA (TCS) stopping calculation of the corresponding electron gas contributions. The results, using the same ELF in the optical limit as a starting point are shown in Fig. 10. For all calculations in this figure the extension of the dielectric function is the same, the differences are due to the non-linear effects only included in the IDA and TCS.

For the IDA method differences with the first-order Penn approach are noticeably around 150 keV and at very low energies. Splitting up the contribution from the 1s and 2s electrons we can more clearly observe non-linear (higher-order) effects, the difference the Penn and IDA curves. For the 2s electrons both curves are very similar except for low energies (E < 10 keV). This means that non-linear effects are of minor importance at high energies for this shell. In addition the standard transport cross section (TCS) method converges very slow to the Penn (and Bethe) results for large E_0 values and therefore it is not able to give properly the first higher-order term (Barkas contribution, proportional to Z^3). At low energies (E < 10 keV) both methods (IDA and TCS) are similar and give a positive Barkas effect. For 1s electrons the Barkas effect is more pronounced at high energies since it depends linearly on the binding energy or resonance frequency of the shell [48]. At low energies, the Barkas effect should be smaller for inner-shells and since, in the framework of FEG, the corresponding Fermi velocity is larger, and hence the FBA is applicable. Overall, considering all electrons, for

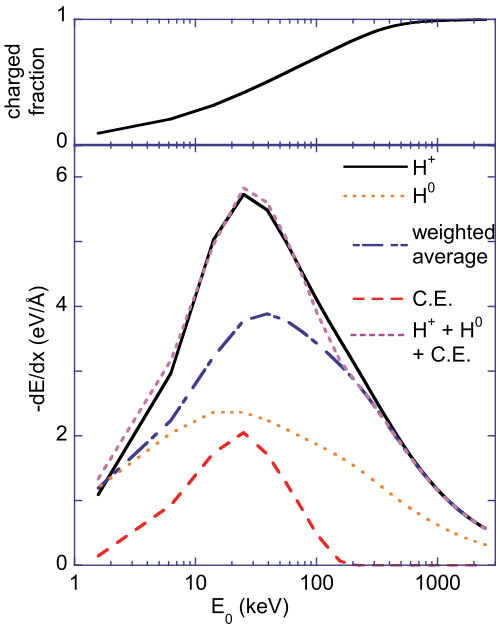

Fig. 11. The effect of the presence of a neutral H fraction for the case of the IDA. The top panel shows the energy dependence of the charged fraction of the projectile. The lower panel stopping for H^+ and H^0 and their weighted average. Charge exchange (C.E.) effects cause additional energy losses. The total stopping for a mixed 1+, neutral beam including C.E. is very close to the pure H^+ stopping.

IDA method differences with the first-order Penn approach are noticeably around 150 keV and at very low energies and are a consequence of the above described shell-wise Barkas effect.

4.3. Neutral fraction and charge exchange effects

For lower energies the approximation of the projectile as a charged particle is poor, as electrons tend to attach to the proton resulting in a neutral projectile of the time. For neutral H (H^0) the interaction with the electron gas is less, especially at larger q values. On the other hand, transition from a charged state to a neutral state and vice versa will induce charge-exchange losses. These effects were investigated for the IDA and the model that is expected to be most appropriate at lower projectile energies. The charged fraction was calculated using the CASP program [49,50]. The stopping for neutral H was implemented as described in Ref. [51], and the charge exchange losses was taken from Ref. [52]. As is clear from Fig. 11 the stopping is reduced due to presence of a H^0 fraction. However, in this case the reduction is almost perfectly cancelled by the additional losses due to charge exchange processes. The almost perfect cancellation could be a consequence of the approximations made. We will not consider the effecs of a neutral fraction and charge exchange in the remainder of this paper.

4.4. Comparison with experimental stopping data

None of the extension schemes is in 100% agreement with the X-ray scattering results. What does this mean for the validity of the derived stopping values? To discuss this we show in Fig. 12 the obtained stopping power and compare it with the limited available experimental results of Bader et al. [31] and Eppacher et al [32] as well as the estimate of the SRIM database [53]. For low projectile energy the valence band contribution dominates and the GOS, truncated $A(q)$ and negative A results, all treat the valence band using the same Mermin function and are thus almost identical. The Penn method results in a somewhat lower stopping, as expected based on the discussion in section 3.1. The IDA results at higher energies ($\approx$ 100 keV) are again very close

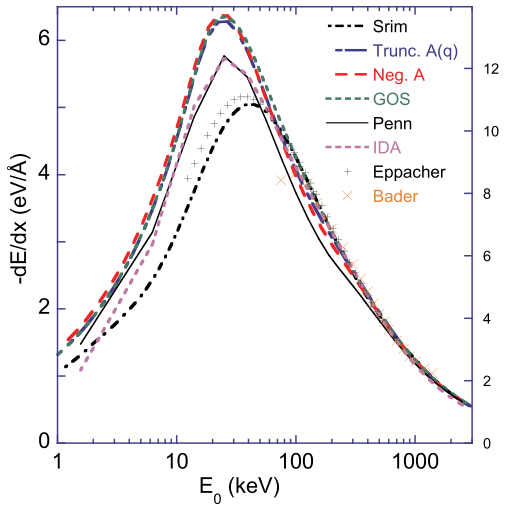

Fig. 12. The top panel shows the stopping values for protons in Li from the various approaches described here, compared to the SRIM estimate and the measurements of Eppacher et al. [32] and Bader et al. [31].

however, to the Mermin results. There are small differences between the GOS, truncated $A(q)$ and negative A methods for E_0 values in the 30–500 keV range, where the stopping due to the 1s electrons has its maximum, but the differences are minor as most of the stopping for these energies is still from the valence band. The differences are too small to distinguish the different approaches based on the measured stopping values. Note however, that below 50 keV the measured stopping by Eppacher et al. [32] is slightly smaller than the calculated ones. This is in spite of the fact that the experimentally observed dispersion is less than the calculated one. Slower dispersion should lead to an earlier onset of the stopping (see Fig. 1).

We have seen how the lithium dielectric function compares to the experiment at various q-values. In order to get some understanding how these observations relate to the calculated stopping power one needs some insight in how much the ELF at momentum q contributes to the stopping for a given projectile energy. For this purpose we plotted how different q values the contribution to the stopping integral (eq. (1)) as a function of E_0 in Fig. 13. The Li modelled using the GOS approach was used here, but similar results would apply to all other approaches. For lower E_0 values the contribution is for q near 0.7 a.u., where the qv line approaches the plasmon branch. At larger E_0 values the range of q that contributes to the stopping is wider with the maximum contribution at decreasing q values. The influence of the core level is first visible near

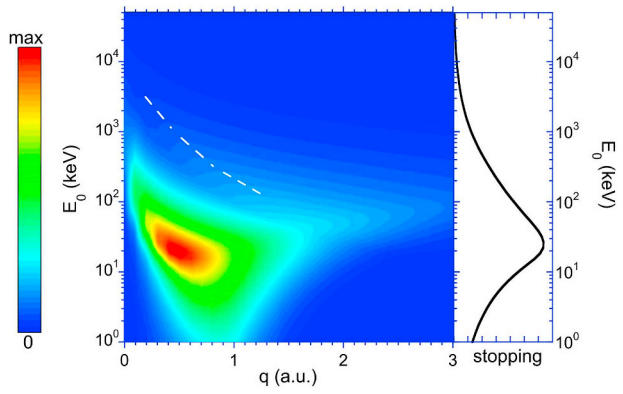

Fig. 13. The distribution of the contribution of the stopping integral (eq. 1) over q as a function of E0. Integrating over q gives the total stopping shown on the right. The valence band was modelled with a Mermin dielectric function. The minimum q for which the 1s electrons (modelled as a GOS) contributes to the stopping is indicated by the dashed line.

$E_0 = 200$ keV at $q \approx 1$ a.u. And extends to lower q values with increasing E_0. Thus below 10 keV it is crucial to get the description of the ELF right for the $0.5 < q < 1$ a.u. Range.

5. Conclusion

We have seen in this paper that the shape of the ELF, as a function of q, varies remarkably depending on the model used to describe the $q-$dependence. However, as all theories are restrained by the Bethe sum rule, the range in stopping values that is obtained is considerably smaller, as high intensities of the loss function for certain ω values are always accompanied by low intensities at other ω values. At large q values the ELF is concentrated along the Bethe ridge and the integration over ω at large q is the same for all models.

At lower energies the charge state of the projectile will affect the stopping and charge exchange effects are important, but both contributions cancelled almost perfectly for the approximations used here. Somewhat surprisingly, for the Li case studied here, deviations from first Born theory, as predicted by the IDA are significant in particular at energies close to the maximum of the stopping contribution of the core electrons.

Having obtained a fair understanding of how the model dielectric function affects the stopping, the question that remains to be answered is which method is preferable, either in general or more specific for stopping calculation. Experimentally, for Li the answer is difficult as there is only one set of data in the interesting projectile energy range, and the comparison is further complicated by charge exchange effects and limitations of the FBA, for which we only can correct approximately within the Penn model. The differences between the various models is smaller than the disagreement with the experiment. The Penn stopping is somewhat smaller at lower energies ($E_0 < 300$ keV) but the IDA corrections beyond the FBA increases the stopping somewhat above 100 keV.

In summary, large deviations can occur where certain levels start contributing to the ELF, and then the dispersion model used is important. When fitting the ELF with Mermin functions the use of Γ_i values of the order of ω_i is probably best avoided, as it tends to lead to larger stopping values.

Acknowledgements

This study was financed in part by the Coordenação de Aperfeioamento de Pessoal de Nvel Superior - Brasil (CAPES) - Finance Code 001, by CNPq and PRONEX-FAPERGS. The authors thank Nestor Arista for helpful comments and a critical reading of the manuscript.

Appendix A. Supplementary data

Supplementary data to this article can be found online at https://doi.org/10.1016/j.jpcs.2019.03.010.

Appendix B

For completeness we show here explicitly that the dispersion relation assumed in eq. (5) indeed leads to the Bethe-like stopping (eq. (4)). The stopping power is given in terms of the ELF as

$$-\frac{dE}{dx} = \frac{2Z^2}{\pi v^2}\int_0^\infty \frac{dq}{q}\int_0^{qv} \omega\, d\omega\, \mathrm{Im}\left[\frac{-1}{\varepsilon(q,\omega)}\right], \tag{14}$$

Where Z is the projectile charge. Assuming the ELF given by the Drude model with a narrow peak ($\Gamma \to 0$) at $\omega_p(q)$ the inner integral of the above equation will be given by the Bethe sum rule Eq. (7) for $\omega_p(q) < qv$ and zero otherwise. Therefore,

$$-\frac{dE}{dx} = \frac{4\pi n Z^2}{v^2}\int_0^\infty \frac{dq}{q}\Theta(qv - \omega(q)), \tag{15}$$

where $\Theta(x)$ is the Heavy-side function. The condition $\omega_p(q) < qv$ is realized by $q_{min} < q < q_{max}$ see Fig. 1. For this case the stopping power reads

$$-\frac{dE}{dx} = \frac{4\pi n Z^2}{v^2}\ln\left(\frac{q_{max}}{q_{min}}\right). \tag{16}$$

For the dispersion relation from Eq. (5) we have $q_{min} = \omega_p/v$ and $q_{max} = 2v$ and therefore we get the Bethe-like formula:

$$-\frac{dE}{dx} = \frac{4\pi n Z^2}{v^2}\ln\left(\frac{2v^2}{\omega_p}\right). \tag{17}$$

The parabola and the straight line in the 'Bethe dispersion' (Eq. (5)) meet at $q_c = \sqrt{2\omega_p}$. The integral can be divided into two parts $q_{min} < q < q_c$ and $q_c < q < q_{max}$.

$$-\frac{dE}{dx} = \frac{4\pi n Z^2}{v^2}\left(\ln\left(\frac{q_{max}}{q_c}\right) + \ln\left(\frac{q_c}{q_{min}}\right)\right). \tag{18}$$

Inspection shows that $q_{max}/q_c = 2v/\sqrt{2\omega_p}$ and $q_c/q_{min} = \sqrt{2\omega_p}/(\omega_p/v)$ are identical. This is an example of the 'equipartition principle' [54] which state that the plasmon and electron-hole excitations contribute equally to the stopping. One can use exactly the same approach to derive an analytical expression for the stopping in the case of simple quadratic dispersion (in the limit of $\Gamma \to 0$). In that case one has to replace simply $q_{\max}$ and $q_{\min}$ by the solutions of $qv = q^2/2 + \omega_p$. One obtains:

$$-\frac{dE}{dx} = \frac{4\pi n Z^2}{v^2}\ln\left(\frac{v + \sqrt{v^2 - 2\omega_p}}{v - \sqrt{v^2 - 2\omega_p}}\right), \tag{19}$$

which should not overestimate the stopping at the stopping maximum as much as the Bethe-like equation does. Also in this case the equipartition principle is fulfilled: $q_{max}/q_c = q_c/q_{min}$ as can be easily verified. Similarly, when using full dispersion the stopping becomes:

$$-\frac{dE}{dx} = \frac{4\pi n Z^2}{v^2}\ln\left(\frac{\sqrt{-\frac{2}{3}E_f + v^2 + \sqrt{\left(\frac{2}{3}E_f - v^2\right)^2 - \omega_p^2}}}{\sqrt{-\frac{2}{3}E_f + v^2 - \sqrt{\left(\frac{2}{3}E_f - v^2\right)^2 - \omega_p^2}}}\right), \tag{20}$$

A similar formula within the static electron gas model (i.e. $E_f = 0$) was given by Sigmund (ref. [4], eq. (5.77)).

References

[1] N. Bohr, On the theory of the decrease of velocity of moving electrified particles on passing through matter, Phylosophical Magazine (1913) 10.
[2] H. Bethe, Zur Theorie des Durchgangs schneller Korpuskularstrahlen durch Materie, Ann. Phys. 397 (3) (1930) 325–400, https://doi.org/10.1002/andp.19303970303 https://doi.org/10.1002/andp.19303970303.
[3] J. Lindhard, On the properties of a gas of charged particles, K. Dan. Vidensk. Selsk. Mat.-Fys. Medd. 28 (8) (1954) 1–57 http://gymarkiv.sdu.dk/MFM/kdvs/mfm%2020-29/mfm-28-8.pdf.
[4] P. Sigmund, Particle Penetration and Radiation Effects, Vol. 151 of Springer Series in Solid-State Sciences, Springer, Berlin, 2006.
[5] M. Nastasi, J. Mayer, J.K. Hirvonen, Ion–solid Interactions, Cambridge University Press, 1996, https://doi.org/10.1017/cbo9780511565007.
[6] H. Nikjoo, S. Uehara, D. Emfietzoglou, Interaction of Radiation with Matter, CRC press, 2012.
[7] H. Nikjoo, D. Emfietzoglou, T. Liamsuwan, R. Taleei, D. Liljequist, S. Uehara, Radiation track, DNA damage and response—a review, Rep. Prog. Phys. 79 (2016) 116601, https://doi.org/10.1088/0034-4885/79/11/116601.
[8] D. Emfietzoglou, R. Garcia-Molina, I. Kyriakou, I. Abril, H. Nikjoo, A dielectric response study of the electronic stopping power of liquid water for energetic protons and a new *i*-value for water, Phys. Med. Biol. 54 (2009) 3451, https://doi.org/10.1088/0031-9155/54/11/012.
[9] D. Emfietzoglou, I. Kyriakou, R. Garcia-Molina, I. Abril, Inelastic mean free path of low-energy electrons in condensed media: beyond the standard models, Surf. Interface Anal. 49 (2017) 4, https://doi.org/10.1002/sia.5878.
[10] J.D. Bourke, C.T. Chantler, Momentum-dependent lifetime broadening of electron energy loss spectra: a self-consistent coupled-plasmon model, J. Phys. Chem. Lett. 6 (2015) 314, https://doi.org/10.1021/jz5023812.
[11] C.T. Chantler, J.D. Bourke, New constraints for low-momentum electronic excitations in condensed matter: fundamental consequences from classical and quantum dielectric theory, J. Phys. Condens. Matter 27 (45) (2015) 455901, https://doi.org/10.1088/0953-8984/27/45/455901.
[12] R. Garcia-Molina, I. Abril, S. Heredia-Avalos, I. Kyriakou, D. Emfietzoglou, A combined molecular dynamics and Monte Carlo simulation of the spatial distribution of energy deposition by proton beams in liquid water, Phys. Med. Biol. 56 (2011) 6475, https://doi.org/10.1088/0031-9155/56/19/019.
[13] R. Garcia-Molina, I. Abril, I. Kyriakou, D. Emfietzoglou, Energy loss of swift protons in liquid water: role of optical data input and extension algorithms, in: G.G. Gomez-Tejedor, M.C. Fuss (Eds.), Radiation Damage in Biomolecular Systems, Springer, 2012.
[14] D. Pines, Elementary Excitations in Solids, Benjamin, New York, 1963.
[15] R.F. Egerton, Electron Energy-Loss Spectroscopy in the Electron Microscope, third ed. Edition, Plenum Press, New York, 2011, https://doi.org/10.1007/978-1-4419-9583-4.
[16] B.I. Lundqvist, Single-particle spectrum of the degenerate electron gas, Physik der Kondensierten Materie 6 (3) (1967) 206, https://doi.org/10.1007/bf02422717.
[17] N. Mermin, Lindhard dielectric function in the relaxation-time approximation, Phys. Rev. B 1 (1970) 2362–2363, https://doi.org/10.1103/physrevb.1.2362.
[18] A.P. Pathak, M. Yussouff, Charged particle energy loss to electron gas, Phys. Status Solidi 49 (1972) 431, https://doi.org/10.1002/pssb.2220490205.
[19] T. Kaneko, Wave-packet theory of stopping of bound electrons, Phys. Rev. 40 (1989) 2188, https://doi.org/10.1103/physreva.40.2188.
[20] I. Abril, R. Garcia-Molina, C. Denton, F. Pérez-Pérez, N. Arista, Dielectric description of wakes and stopping powers in solids, Phys. Rev. 58 (1998) 357, https://doi.org/10.1103/physreva.58.357.
[21] C. Tung, J. Ashley, R. Ritchie, Electron inelastic mean free paths and energy losses in solids ii: electron gas statistical model, Surf. Sci. 81 (2) (1979) 427, https://doi.org/10.1016/0039-6028(79)90110-9.
[22] D. Penn, Electron mean-free-path calculations using a model dielectric function, Phys. Rev. B 35 (1987) 482, https://doi.org/10.1103/PhysRevB.35.482.
[23] B. Da, H. Shinotsuka, H. Yoshikawa, S. Tanuma, Comparison of the mermin and penn models for inelastic mean-free path calculations for electrons based on a model using optical energy-loss functions, Surf. Interface Anal. in presss. doi:10.1002/sia.6628.
[24] S. Heredia-Avalos, R. Garcia-Molina, J.M. Fernández-Varea, I. Abril, Calculated energy loss of swift He, Li, B, and N ions in SiO_2, Al_2O_3, and ZrO_2, Phys. Rev. 72 (2005) 052902, https://doi.org/10.1103/physreva.72.052902.
[25] M. Vos, P.L. Grande, Modeling the contribution of semi-core electrons to the dielectric function, J. Phys. Chem. Solids 124 (2019) 242, https://doi.org/10.1016/j.jpcs.2018.09.020.
[26] B. Da, H. Shinotsuka, H. Yoshikawa, Z.J. Ding, S. Tanuma, Extended Mermin method for calculating the electron inelastic mean free path, Phys. Rev. Lett. 113 (2014) 063201, https://doi.org/10.1103/physrevlett.113.063201.
[27] Y. Sun, H. Xu, B. Da, S. feng Mao, Z. jun Ding, Calculations of energy-loss function for 26 materials, Chin. J. Chem. Phys. 29 (2016) 663, https://doi.org/10.1063/1674-0068/29/cjcp1605110.
[28] C.C. Montanari, J.E. Miraglia, Low- and intermediate-energy stopping power of protons and antiprotons in solid targets, Phys. Rev. 96 (2017) 012707, https://doi.org/10.1103/physreva.96.012707.
[29] Z. Levine, S. Louie, New model dielectric function and exchange-correlation potential for semiconductors and insulators, Phys. Rev. B 25 (1982) 6310, https://doi.org/10.1103/physrevb.25.6310.
[30] M. Vos, P. Grande, Simple model dielectric functions for insulators, J. Phys. Chem. Solids 104 (2017) 192, https://doi.org/10.1016/j.jpcs.2016.12.015.
[31] M. Bader, R.E. Pixley, F.S. Mozer, W. Whaling, Stopping cross section of solids for protons, 50-600 kev, Phys. Rev. 103 (1956) 32–33, https://doi.org/10.1103/physrev.103.32.
[32] C. Eppacher, R.D. Muiño, D. Semrad, A. Arnau, Stopping power of lithium for hydrogen projectiles, Nucl. Instrum. Methods Phys. Res., Sect. B 96 (1995) 639, https://doi.org/10.1016/0168-583x(95)00258-8.
[33] R.J. Mathar, J.R. Sabin, S.B. Trickey, Electronic stopping of protons for lithium in the dielectric formulation obtained from first-principles calculations, Nucl. Instrum. Methods Phys. Res., Sect. B 155 (1999) 249, https://doi.org/10.1016/s0168-583x(99)00295-5.
[34] R. Cabrera-Trujillo, J.R. Sabin, E. Deumens, Y. hrn, Cross sections for H^+ and H atoms colliding with Li in the low keV energy region, Phys. Rev. 78 (2008) 012707, https://doi.org/10.1103/physreva.78.012707.
[35] H. Nagasawa, S. Mourikis, W. Schülke, X-Ray Raman spectrum of Li, Be and graphite in a high-resolution inelastic synchrotron X-ray scattering experiment, J. Phys. Soc. Jpn. 58 (1989) 710, https://doi.org/10.1143/jpsj.58.710.
[36] H. Nagasawa, S. Mourikis, W. Schülke, Momentum-transfer dependence of the near edge structure of Li, J. Phys. Soc. Jpn. 66 (10) (1997) 3139–3146, https://doi.org/10.1143/jpsj.66.3139.
[37] K.J. Chen, V. Caspar, C. Bellin, G. Loupias, Investigation of temperature dependence of Compton profiles in lithium, Solid State Commun. 110 (1999) 357, https://doi.org/10.1016/s0038-1098(99)00094-0.
[38] M. Rasigni, G. Rasigni, Optical constants of lithium deposits as determined from the Kramers-Kronig analysis, J. Opt. Soc. Am. 67 (1977) 54, https://doi.org/10.1364/josa.67.000054.
[39] T. Kloos, Plasmaschwingungen in Al, Mg, Li, Na und K angeregt durch schnelle Elektronen, Zeitschrift fr Physik A Hadrons and nuclei 265 (1973) 225, https://doi.org/10.1007/bf01397716.
[40] B. Henke, E. Gullikson, J. Davis, X-ray interactions: photoabsorption, scattering, transmission, and reflection at E = 50-30,000 eV, Z = 1-92, Atomic Data Nucl. Data Tables 54 (1993) 181, https://doi.org/10.1006/adnd.1993.1013.
[41] J.C. Slater, Atomic shielding constants, Phys. Rev. 36 (1930) 57, https://doi.org/10.1103/physrev.36.57.
[42] M.J. Cooper, Compton scattering and electron momentum determination, Rep. Prog. Phys. 48 (1985) 415–481, https://doi.org/10.1088/0034-4885/48/4/001.
[43] F. Biggs, L. Mendelsohn, J. Mann, Hartree-Fock Compton profiles for the elements, Atomic Data Nucl. Data Tables 16 (1975) 201, https://doi.org/10.1016/0092-640x(75)90030-3.
[44] W. Schülke, G. Stutz, F. Wohlert, A. Kaprolat, Electron momentum-space density of Li metal a high-resolution compton-scattering study, Phys. Rev. B 54 (1996) 14381.
[45] I. Nagy, A. Bergara, A model for the velocity-dependent screening, Nucl. Instrum. Methods Phys. Res., Sect. B 115 (1996) 58, https://doi.org/10.1016/0168-583x(96)01562-5.
[46] W.H. Barkas, W. Birnbaum, F.M. Smith, Mass-ratio method applied to the measurement of *l*-meson masses and the energy balance in pion decay, Phys. Rev. 101 (1956) 778–795, https://doi.org/10.1103/PhysRev.101.778.
[47] P. L. Grande, Alternative treatment for the energy-transfer and transport cross section in dressed electron-ion binary collisions, Phys. Rev. 94. doi:10.1103/physreva.94.042704.
[48] J. Lindhard, The Barkas effect - or Z_1^3, Z_1^4-corrections to stopping of swift charged particles, Nucl. Instrum. Methods 132 (0) (1976) 1–5 https://doi.org/10.1016/0029-554X(76)90702-3.
[49] P. Grande, G. Schiwietz, CasP Program, (2001) http://www.casp-program.org/ http://www.casp-program.org/.
[50] G. Schiwietz, K. Czerski, M. Roth, F. Staufenbiel, P. Grande, Femtosecond dynamics snapshots of the early ion-track evolution, Nucl. Instrum. Methods Phys. Res., Sect. B 226 (2004) 683, https://doi.org/10.1016/j.nimb.2004.05.043.
[51] R. Garcia-Molina, S. Heredia-Avalos, I. Abril, Molecular structure effects in the energy loss of swift boron molecular ions in solids, J. Phys. Condens. Matter 12 (2000) 5519, https://doi.org/10.1088/0953-8984/12/25/315.
[52] G. Schiwietz, P.L. Grande, Introducing electron capture into the unitary-convolution-approximation energy-loss theory at low velocities, Phys. Rev. 84 (2011) 052703, https://doi.org/10.1103/physreva.84.052703.
[53] J.F. Ziegler, SRIM-2003, Nucl. Instrum. Methods Phys. Res., Sect. B 219–220 (2004) 1027, https://doi.org/10.1016/j.nimb.2004.01.208.
[54] J. Lindhard, A. Winther, Stopping power of electron gas and equipartition rule, Mat Fys Medd Dan Vid Selsk 34 (1964) 1 http://gymarkiv.sdu.dk/MFM/kdvs/mfm%2030-39/mfm-34-4.pdf.